

ORIGINAL ARTICLE

$K_4CaSi_6O_{15}$ —Solving a 90-year-old riddle

Hang Liu  | Elias Hildebrandt | Hans Krammer | Volker Kahlenberg  |
Hannes Krüger  | Herwig Schottenberger 

Institute of Mineralogy and Petrography,
University of Innsbruck, Innsbruck,
Austria

Correspondence

Institute of Mineralogy and Petrography,
University of Innsbruck, Innrain 52, A-
6020 Innsbruck, Austria.

Email: volker.kahlenberg@uibk.ac.at

Funding information

Austrian Science Fund, Grant/Award
Number: P30754

Abstract

Polycrystalline $K_4CaSi_6O_{15}$ was prepared from (a) solid-state reactions between stoichiometric mixtures of the corresponding oxides/carbonates and (b) combustion solution synthesis using K- and Ca-nitrates, tetraethyl orthosilicate (TEOS), and glycine (fuel component) as starting reagents. The compound was characterized by powder X-ray diffraction. Differential thermal analysis indicated that $K_4CaSi_6O_{15}$ melts congruently at about 956°C. On cooling down from the liquid state, a distinct glass-forming tendency was observed. Single crystals suitable for further structural investigations were obtained from sinter experiments just below the melting point. Basic crystallographic data are as follows: monoclinic symmetry, space group Pc , $a = 6.9299(2)$ Å, $b = 27.3496(9)$ Å, $c = 12.2187(4)$ Å, $\beta = 93.744(3)^\circ$, $V = 2310.86(13)$ Å³, $Z = 3$. The crystal structure of $K_4CaSi_6O_{15}$ belongs to the group of interrupted framework silicates with exclusively Q^3 -units. The tetrahedral network is the first inorganic representative of the so-called *eth*-type. Charge compensation in the structure is achieved by the incorporation of potassium and calcium cations, which are coordinated by five to nine oxygen ligands. Ninety years after its first mention the present contribution proves the existence of $K_4CaSi_6O_{15}$ as a stable phase in the ternary system K_2O – CaO – SiO_2 .

KEYWORDS

crystal structure, $K_4CaSi_6O_{15}$, K_2O – CaO – SiO_2 system, potassium calcium silicate, solution combustion synthesis

1 | INTRODUCTION

In their landmark paper from 1930, Morey, Kracek, and Bowen¹ published a detailed study on the liquidus and sub-solidus phase relationships in the ternary system K_2O – CaO – SiO_2 . The authors reported a total of six different crystalline phases: $K_2Ca_2Si_9O_{21}$, $K_8CaSi_{10}O_{25}$, $K_4CaSi_6O_{15}$, $K_2Ca_3Si_6O_{16}$, $K_4CaSi_3O_9$, and K_2CaSiO_4 , respectively. The description of the experimental details clearly indicates that this early study has been performed

with great care and that the results can principally serve as a basis for the interpretation of the phase diagram. Nevertheless, this investigation has several weak points which are attributable to the limited analytical tools available in the 1930s. First of all, the chemical formulas of the crystalline phases were estimated from the starting composition of the glasses or from the initial weight fractions of the educts, that is, no chemical analysis of the products has been performed. Second, the only other characterization method of the crystals was the determination of their

This is an open access article under the terms of the Creative Commons Attribution License, which permits use, distribution and reproduction in any medium, provided the original work is properly cited.

© 2021 The Authors. *Journal of the American Ceramic Society* published by Wiley Periodicals LLC on behalf of American Ceramic Society (ACERS)

optical properties including measurements of the refractive indices. Optical features also served to establish hypotheses concerning the crystal systems, that is, neither powder/single-crystal diffraction nor spectroscopic data have been collected.

Our own studies performed during the last years arouse suspicion not only with respect to the number of crystalline phases that have been previously described in the literature, but also concerning their chemical composition. In summary one can state that (a) some of the phases mentioned by Morey and co-authors¹ do exist ($K_8CaSi_{10}O_{25}$ and $K_4CaSi_3O_9$),^{2,3} (b) some have slightly different chemical compositions ($K_2Ca_2Si_8O_{19}$),⁴ (c) several crystalline compounds have been overlooked in the previous study ($K_2Ca_2Si_2O_7$, $K_2Ca_3Si_3O_{10}$, $K_2Ca_6Si_4O_{15}$, $K_2CaSi_4O_{10}$)⁵⁻⁸ and (d) at least one compound (K_2CaSiO_4)⁹ has to be disconfirmed. Furthermore, extensive solid solutions among the potassium calcium silicates seem to be virtually absent. From a structural point of view, this is probably due to the pronounced differences in the ionic radii between K^+ and Ca^{2+} ($r_K^{[6]}$: 1.38 Å, $r_{Ca}^{[6]}$: 1.00 Å).¹⁰

Given that the compounds of the system K_2O – CaO – SiO_2 can occur in a variety of residual materials, a comprehensive understanding of the equilibria between the existing phases is not only of interest for fundamental research, but also from an applicative point of view. Prominent classes of the relevant recycling materials are different types of ashes and slags occurring in a number of industrial combustion, gasification, pyrolysis, and metallurgical processes.¹¹⁻¹⁶ Moreover, the ternary system is also important for the interpretation of the properties and manufacturing of technical, as well as ancient glasses.¹⁷⁻²⁰ Furthermore, detailed knowledge concerning the solid-state characteristics of the existing crystalline compounds occurring in the system K_2O – CaO – SiO_2 is of the essence for the identification of these phases in technical products.^{16,21-23} Likewise, the results from experimental phase analytical studies represent an indispensable input for any kind of thermodynamic modeling including database development for slag-relevant oxides.²⁴⁻²⁷

In the course of our ongoing project to unravel the number of crystalline phases in the system K_2O – CaO – SiO_2 , we found evidence that the so-called 2:1:6 phase ($K_4CaSi_6O_{15}$) reported by Morey et al.¹ may, indeed, represent a valid and relevant composition for an existing potassium calcium silicate.²⁸ Therefore, we tried to synthesize this phase in pure form using (a) classical solid-state reactions between oxides and (b) the solution combustion method. Finally, the present paper reports a detailed crystallographic description of the compound.

2 | EXPERIMENTAL DETAILS

2.1 | Synthesis

First synthetic experiments for the preparation of polycrystalline $K_4CaSi_6O_{15}$ were based on solid-state reactions. Thus,

a mixture of K_2CO_3 (Alfa Aesar, 99.997%), $CaCO_3$ (Merck, min. 99%), and amorphous SiO_2 (Alfa Aesar, 99.995%) in the molar ratio of 2:1:6 was homogenized under ethanol in a planetary ball mill using an agate jar. Prior to weighing, the educts were dried for several hours at 300°C to eliminate possible hydrated phases such as $K_2CO_3 \cdot 1.5H_2O$ or physically adsorbed water. The homogenized slurry was dried at 50°C for 12 h and, subsequently, the material was pressed into pellets having a weight of about 0.5 g and a diameter of 12 mm. The tablets were wrapped into Pt-foil in order to reduce losses of the K_2O -component upon heating and placed in an alumina combustion boat. Firing was performed in a resistance heated tube furnace from room temperature to 950°C applying a heating ramp of 50°C/h—just below the melting point of 959°C reported by Morey et al.¹ After annealing for 13 h at the target temperature the samples were removed from the furnace (sample Ia). Parts of the porous white solid pellets were pulverized in an agate mortar for further characterization using PXRD. In a second experiment (sample Ib), annealing at 950°C was followed by slow cooling with 10°C/h down to room temperature. This sample contained single crystals of sufficient quality for complete crystal structure analysis.

As an alternative method for the preparation of polycrystalline $K_4CaSi_6O_{15}$, we tested the applicability of the well-known solution combustion synthesis (SCS). SCS is based on a fast and self-sustained redox reaction between a fuel and an oxidant in the presence of metal cations.²⁹ Frequently, oxidants consist of the metal precursor salts in their own, such as metal nitrates. The fuel components usually belong to organic species, for example, glycine, alanine or gluconate anions. Principally, SCS requires three major steps: (a) formation of the stoichiometric reaction mixture (with respect to the final metal ratios), (b) hydrolytic formation of a precursor gel, and (c) combustion of the gel.²⁹ Upon thermally induced self-ignition a highly reactive, porous, and amorphous, almost homogeneous matrix is formed. The matrix requires a final calcination step for (a) removing volatile components and (b) eventually yielding the desired polycrystalline compounds.

For the synthesis of the present compound, the pH of 40 ml of distilled water was adjusted to 1 with 0.28 ml of nitric acid (65%). Potassium nitrate (6.07 g, Alfa Aesar 99%), 3.45 g calcium nitrate tetrahydrate (Merck 99%), and 3.38 g glycine (Merck) were dissolved and transferred into a 200 ml heavy walled, tube-shaped Schlenk bomb. Twenty milliliters of tetraethyl orthosilicate (TEOS, Merck) was added with a syringe. In order to raise the solubility of TEOS and to speed up the hydrolysis reaction, 20 ml of ethanol was added and the glass vessel was finally placed in an ultrasonic bath. After 12 h a turbid gel had formed that was subsequently transferred into a beaker with about 80 ml of ethanol, stirred at

80°C to remove surplus fluid, and finally kept for 12 h at 120°C in a drying cabinet. The resulting xerogel was crushed and transferred into a mullite-based ceramic crucible, which was placed in an open muffle furnace. The oven was covered with a metal cap to confine ash-like flakes that occurred during the self-combustion reaction which started at about 180°C approximately 15 min after launching the heating. The resulting light-grey porous mass was homogenized in an agate mortar and pressed into pellets of about 0.5 g. In a first heat treatment the pellets were fired in a chamber furnace to 600°C in order to remove the nitrate and carbon residues (ramp: 50°C/min; dwell time: 24 h) and quenched in air. The white, X-ray amorphous product was re-ground, pressed again, and annealed at 850°C under otherwise identical conditions (sample II).

2.2 | Powder diffraction

Powder diffraction data for samples I and II were acquired on a Bruker D8-Discover diffractometer using a Cu-tube operated at 40 kV and 40 mA. The device is equipped with a primary beam Ge-monochromator and a LYNXEYETM silicon strip detector. Data were collected in Bragg-Brentano θ - 2θ geometry at ambient temperature in the range between 3 and 70° 2θ with a counting time of 7 s per step and a total of 6335 steps resulting in a 2θ -resolution of about 0.01°. A fixed 0.3° divergence slit, as well as primary and secondary Soller slits were used. The samples were prepared on a “background-free” sample holder consisting of the polished surface of a specially cut silicon single crystal.

Qualitative phase analysis was attempted with the 2018 release of the PDF-4 Powder Diffraction File issued by the International Centre for Diffraction Data.³⁰ However, it was not possible to allocate the peaks to any single phase or mixture of phases listed in this database. Figure 1 shows the corresponding diffractograms of samples Ia and II. They indicate that both aforementioned synthesis routes resulted in the same phase content. Fortunately, the fragments from the solid-state reactions (sample Ia) contained at least low-quality colorless optically transparent crystals that could be used for a preliminary determination of the unit-cell parameters using single-crystal X-ray diffraction. The resulting monoclinic primitive metric satisfactorily explained the powder diffraction patterns proving the single-phase character of the material, whose composition turned out to be $\text{K}_4\text{CaSi}_6\text{O}_{15}$ (see crystal structure analysis). Figure 2 shows a LeBail-fit of the data acquired for sample Ia using the program FullProf2.k³¹ in combination with the WinPLOTR graphical interface.³² The background was determined by linear interpolation between a set of breakpoints with refinable heights. Intensities within eight times the full width at half maximum of a peak were considered to contribute to the central reflection. Pseudo-Voigt functions were chosen for the simulation of the peak shape with two parameters defining the Lorentzian and Gaussian character as a function of 2θ . Furthermore, an asymmetry correction following the procedure of Finger et al.³³ was included. The angular variation of the line width was accounted for using the Cagliotti function. Final background-corrected profile residuals were $R_p = 0.149$ and $R_{wp} = 0.158$, respectively. The

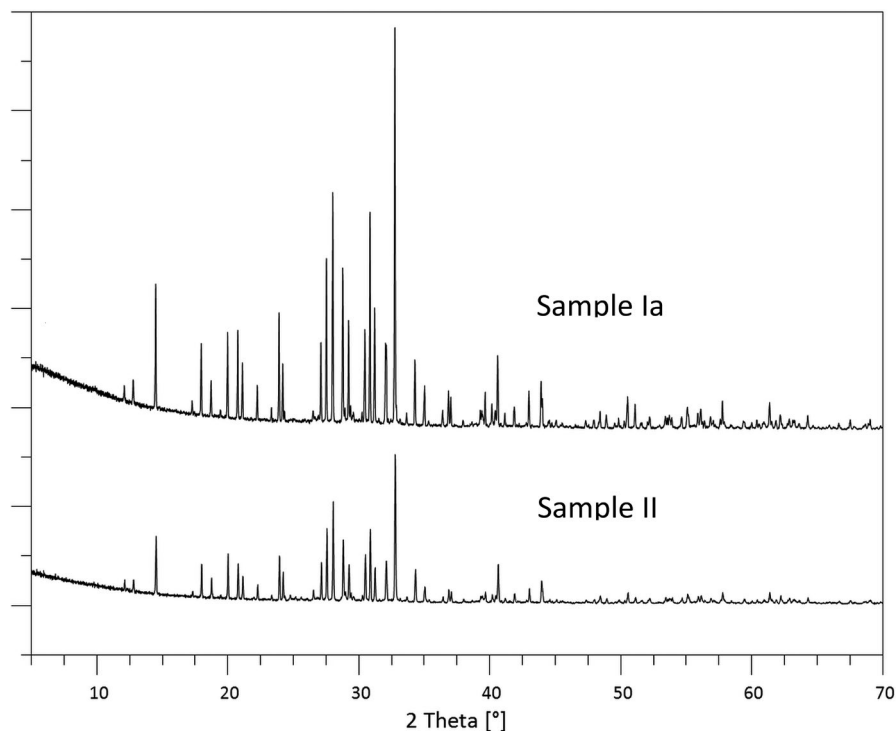


FIGURE 1 Comparison between the powder diffraction patterns of polycrystalline $\text{K}_4\text{CaSi}_6\text{O}_{15}$ prepared by solid-state reactions (sample Ia) and solution combustion synthesis (sample II). For sake of clarity, the diffractogram of sample Ia has been shifted along the ordinate

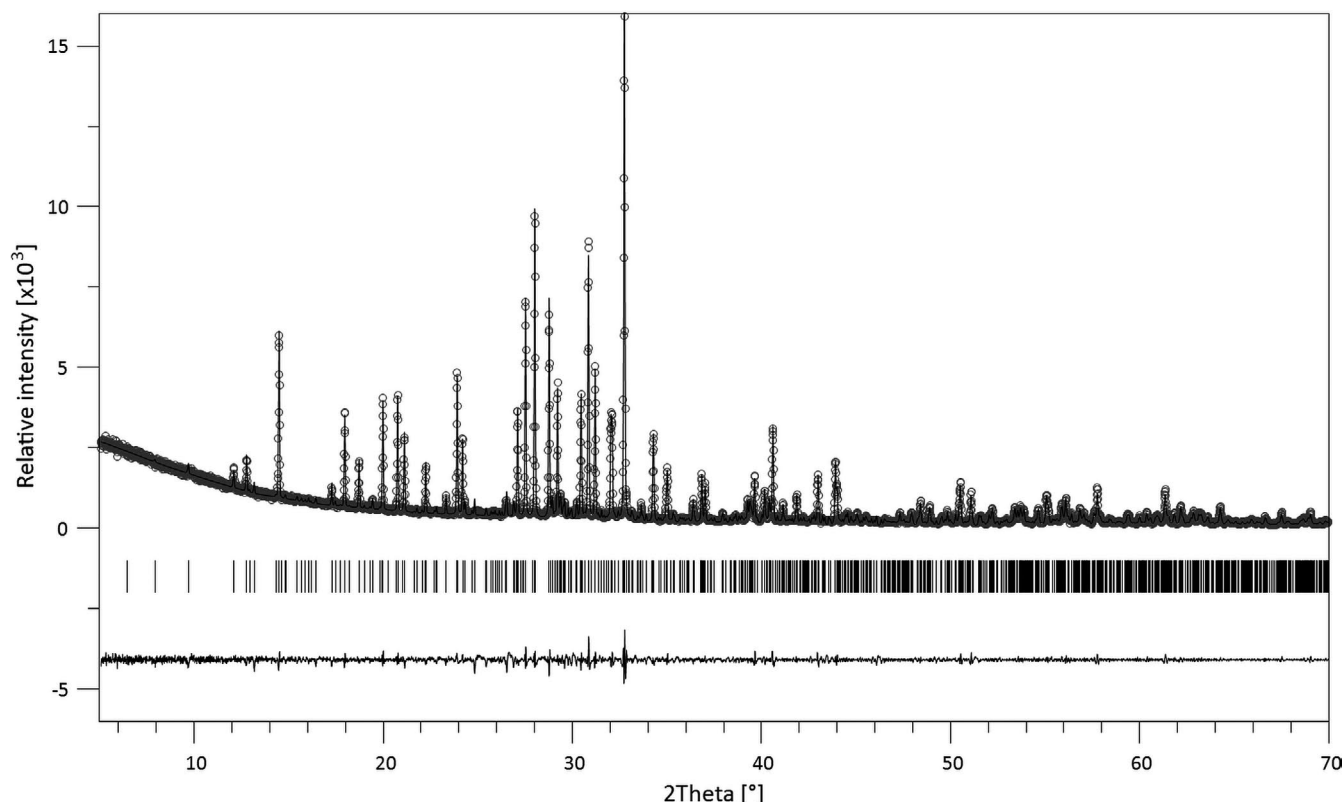


FIGURE 2 LeBail-fit of the powder diffraction pattern acquired for sample Ia prepared by solid-state reactions at 950°C (Cu-K α_1 radiation). Observed step intensities, y_o , are represented by small circles. Calculated step intensities y_c (solid line) have been modeled based on a monoclinic primitive unit cell and space group Pc (see text). Tick marks for the Bragg peaks are given. The lower line shows the difference curve between observed and calculated step intensities, $y_o - y_c$

resulting lattice parameters are as follows: $a = 6.94277(4)$ Å, $b = 27.3938(2)$ Å, $c = 12.14455(7)$, $\beta = 93.7291(3)^\circ$. These values compare reasonably well with the ones obtained in the single-crystal diffraction study. At any rate, the standard uncertainties of the lattice parameters are significantly higher than those listed above, which have been obtained from the fitting software and reflect only the precision of the mathematical fit between measured and calculated step intensities.

2.3 | Thermal analysis

DTA and TG measurements of 56.1 mg of polycrystalline phase pure $K_4CaSi_6O_{15}$ were conducted employing simultaneous differential thermal and thermogravimetric analysis (DTA-TGA). The experiment was performed in air using a Setaram SETSYS Evolution 2400 thermal apparatus using a TGA-DTA 1600 sample holder equipped with Pt/Pt90-Rh10 thermocouples and 100 μ l Pt-crucibles. The applied temperature program consisted of a heating segment (5°C/min heating rate) and subsequent cooling to room temperature using the same rate.

2.4 | Single-crystal diffraction

For detailed structural investigations at ambient conditions, a crystal of good optical quality from sample Ib was mounted on the tip of glass fiber using nail polish. X-ray diffraction data collection at 23°C was performed with an Oxford Diffraction Gemini R Ultra single-crystal diffractometer using Mo-K α radiation. A total of 892 frames using ω -scans with 1.0° scan width per frame and 60 s exposure time covering a full sphere of reciprocal space was collected. Integration and data reduction were performed using the CrysAlis Pro software package (Rigaku Oxford Diffraction 2020)³⁴ including the corrections for Lorentz- and polarization effects. The intensities were also corrected for absorption with 13 indexed faces describing the morphology of the irregular fragment used for data collection.

Analysis of the diffraction symmetry pointed to the monoclinic Laue group $2/m$. Systematic absences suggested two possible space group: Pc or $P2/c$. Furthermore, superstructure effects were present, that is, the average intensity, $\langle I_{hkl} \rangle$, of the reflections with $l = 3n$ was about twice as large as the value for the class with $l \neq 3n$.

Structure determination was initiated in both space groups by direct methods implemented in the program SIR2004.³⁵

However, only for the non-centrosymmetric case, a crystallochemically reasonable partial structure could be obtained that was successfully completed with difference Fourier calculations. The derived model was consistent with the molar oxide ratio $\text{K}_2\text{O}:\text{CaO}:\text{SiO}_2$ of 2:1:6. A single unit cell contains three formula units of $\text{K}_4\text{CaSi}_6\text{O}_{15}$. Subsequent least-squares refinements were performed using the program SHELX-97³⁶ embedded in the WinGX program suite.³⁷ X-ray scattering factors for neutral atoms together with real and imaginary coefficients for anomalous dispersion were taken from the International Tables for Crystallography, Vol. C.³⁸ Analysis of the Bijvoet differences was employed to determine the absolute configuration of the acentric compound. The Flack parameter³⁹ indicated the presence of twinning by inversion which was accounted for in the refinements. Within a tolerance of 0.5 Å, the inspection of the final fractional atomic coordinates using the ADDSYM algorithm implemented in the program PLATON⁴⁰ did not reveal any indication for unnecessarily low space group symmetry. As will be outlined in the results section, four of the potassium cations in the asymmetric unit occupy split positions. During the refinements, it was assumed that the sum of the occupancy factors of the corresponding pairs is 1.0. Furthermore, the anisotropic displacement parameters of the split atom pairs were restrained to be similar (SIMU command of the SHELX-97 program). Final calculations including fractional atomic coordinates and anisotropic displacement factors for all atoms converged to a residual value of $R1 = 0.0326$. Further information concerning data collection and refinement parameters are given in Table 1. In Table 2, fractional atomic coordinates together with equivalent isotropic displacement factors and bond valence sums (BVS) are listed. Selected bond distances and bond angles, polyhedral distortion parameters (λ , σ^2)⁴¹ as well as anisotropic displacement factors are reported in Tables 3 and 4, respectively. For calculating bond valence sums the program ValList⁴² was applied in combination with the parameter sets of Brown and Altermatt⁴³ for Ca–O and K–O as well as Brese and O'Keeffe⁴⁴ for Si–O bonds. Drawings of the crystal structure have been prepared using the program VESTA 3.⁴⁵

3 | RESULTS

3.1 | Thermal analysis

The results of the thermal analysis experiment can be summarized as follows. Upon heating, only one sharp and very intense endothermal effect (onset: 956°C, peak maximum: 968°C) was observed. This signal is related to the congruent melting of the sample. The value compares reasonably well with the melting point of 959°C reported by Morey et al.¹ When cooled down to room temperature, at least under the

TABLE 1 Crystal data and structure refinement for $\text{K}_4\text{CaSi}_6\text{O}_{15}$

Empirical formula	$\text{K}_4\text{CaSi}_6\text{O}_{15}$	
Formula weight	605.02 g/mol	
Temperature	293(2) K	
Wavelength	0.71073 Å	
Crystal system	Monoclinic	
Space group	Pc	
Unit cell dimensions	$a = 6.9299(2)$ Å	$\alpha = 90^\circ$
	$b = 27.3496(9)$ Å	$\beta = 93.744(3)^\circ$
	$c = 12.2187(4)$ Å	$\gamma = 90^\circ$
Volume	2310.86(13) Å ³	
Z	3	
Density (calculated)	2.609 Mg/m ³	
Absorption coefficient	2.035 mm ⁻¹	
F(000)	1800	
Crystal size	0.12 × 0.17 × 0.23 mm ³	
Theta range for data collection	1.489° – 25.348°	
Index ranges	–8 ≤ h ≤ 8, –32 ≤ k ≤ 32, –14 ≤ l ≤ 14	
Reflections collected	31916	
Independent reflections ($I > 2\sigma(I)$)	8453 [$R_{\text{int}} = 0.0337$]	
Completeness to $\theta = 25.242^\circ$	100.0%	
Refinement method	Full-matrix least-squares on F^2	
Data / restraints / parameters	8453/26/744	
Goodness-of-fit on F^2	1.014	
Final R indices ($I > 2\sigma(I)$)	$R1 = 0.0326$, $wR2 = 0.0829$	
R indices (all data)	$R1 = 0.0356$, $wR2 = 0.0853$	
Largest diff. peak and hole	0.545 and –0.588 e.Å ⁻³	

given experimental cooling rates no corresponding exothermal crystallization effect could be detected. After the DTA-run, the sample was recovered from the Pt-crucible. An optical inspection under a polarizing binocular revealed the presence of glass.

3.2 | Crystal structure

The crystal structure of $\text{K}_4\text{CaSi}_6\text{O}_{15}$ is based on a three-dimensional network of $[\text{SiO}_4]$ -tetrahedra where every tetrahedron has one non-bridging (O_{nbr}) and three bridging (O_{br}) oxygen atoms. The resulting interrupted framework

TABLE 2 Atomic coordinates ($\times 10^4$) and equivalent isotropic displacement parameters ($\text{\AA}^2 \times 10^3$) for $\text{K}_4\text{CaSi}_6\text{O}_{15}$. $U(\text{eq})$ is defined as one-third of the trace of the orthogonalized U_{ij} tensor. Bond valence sums (BVS) for the cations are given in valence units (v.u.). All atoms reside in general positions. K51, K52, K61, K62, K71, K72, K111, and K112 correspond to partially occupied split positions (see text)

	Occupancy	<i>x</i>	<i>y</i>	<i>z</i>	<i>U</i> (eq)	BVS
Ca(1)		24(2)	2489(1)	64(1)	8(1)	1.99
Ca(2)		446(3)	5833(1)	9859(2)	10(1)	1.99
Ca(3)		710(2)	9156(1)	9831(1)	10(1)	2.03
K(1)		8603(3)	6557(1)	3240(2)	17(1)	1.21
K(2)		1968(3)	8524(1)	7006(2)	20(1)	0.87
K(3)		2039(3)	4860(1)	1769(2)	22(1)	1.00
K(4)		2015(3)	8192(1)	1602(2)	18(1)	1.34
K(51)	0.40(4)	5560(40)	8250(13)	4684(8)	64(9)	0.77
K(52)	0.60(4)	4947(9)	8007(5)	4730(5)	30(2)	1.05
K(61)	0.61(4)	5720(30)	9762(7)	186(13)	34(3)	0.88
K(62)	0.39(4)	5320(30)	9860(30)	110(30)	58(8)	0.74
K(71)	0.60(6)	5536(14)	6388(8)	136(7)	37(3)	0.98
K(72)	0.40(6)	4970(30)	6599(18)	153(11)	58(9)	0.72
K(8)		8584(3)	6844(1)	7920(2)	20(1)	0.87
K(9)		4898(4)	6808(2)	5248(2)	65(1)	0.88
K(10)		5599(3)	8534(1)	9586(2)	31(1)	1.00
K(111)	0.41(7)	5800(30)	5050(20)	9606(16)	48(8)	0.75
K(112)	0.59(7)	5359(15)	5237(8)	9632(13)	31(3)	0.91
K(12)		9125(3)	179(1)	7927(2)	30(1)	0.88
Si(1)		7781(3)	8690(1)	2129(2)	10(1)	4.17
Si(2)		7620(3)	4591(1)	7180(2)	10(1)	4.20
Si(3)		3470(3)	7381(1)	7571(2)	9(1)	4.10
Si(4)		2854(3)	7058(1)	2731(2)	7(1)	4.27
Si(5)		9781(3)	6206(1)	5795(2)	9(1)	4.20
Si(6)		1116(3)	5467(1)	4028(2)	9(1)	4.27
Si(7)		9444(3)	7110(1)	827(2)	7(1)	4.20
Si(8)		3584(3)	9661(1)	7556(2)	11(1)	4.18
Si(9)		7088(3)	7995(1)	7326(2)	7(1)	4.10
Si(10)		7014(3)	5689(1)	7325(2)	11(1)	4.10
Si(11)		681(3)	7874(1)	9105(2)	7(1)	4.14
Si(12)		4028(3)	9206(1)	2445(2)	11(1)	4.15
Si(13)		7303(3)	9112(1)	7275(2)	10(1)	4.08
Si(14)		6638(3)	7598(1)	2428(2)	9(1)	4.06
Si(15)		1188(3)	8741(1)	4033(2)	10(1)	4.14
Si(16)		154(3)	9550(1)	5678(2)	11(1)	4.18
Si(17)		3908(3)	5966(1)	2431(2)	10(1)	4.21
Si(18)		3373(3)	6273(1)	7574(2)	11(1)	4.17
O(1)		9117(9)	6654(2)	78(5)	18(1)	
O(2)		7544(9)	7253(2)	1490(5)	18(1)	
O(3)		8706(8)	6687(2)	5452(5)	16(1)	
O(4)		3134(8)	9360(2)	8596(5)	21(1)	
O(5)		2857(10)	6036(3)	8670(6)	31(2)	
O(6)		8836(10)	8002(2)	8273(7)	26(2)	

(Continues)

TABLE 2 (Continued)

Occupancy	x	y	z	U(eq)	BVS
O(7)	6624(8)	8171(2)	2042(5)	17(1)	
O(8)	5307(8)	7736(2)	7929(5)	16(1)	
O(9)	1927(9)	7454(2)	8500(6)	21(1)	
O(10)	6363(8)	9104(2)	2606(5)	18(1)	
O(11)	6424(8)	5113(2)	7199(5)	18(1)	
O(12)	9895(10)	7610(2)	177(6)	23(1)	
O(13)	8559(9)	8836(2)	1007(5)	23(1)	
O(14)	3020(9)	5854(2)	1253(6)	22(1)	
O(15)	4333(8)	7468(2)	2310(6)	20(1)	
O(16)	3239(8)	9124(2)	1232(5)	21(1)	
O(17)	9381(10)	4622(3)	8123(7)	34(2)	
O(18)	1867(8)	8349(2)	9406(5)	12(1)	
O(19)	8719(8)	9175(2)	6255(5)	22(1)	
O(20)	2095(9)	7172(2)	3874(5)	24(2)	
O(21)	5014(8)	5973(2)	6924(5)	22(1)	
O(22)	2607(10)	7494(2)	6386(6)	24(2)	
O(23)	5596(8)	9516(2)	7003(5)	23(1)	
O(24)	7532(9)	7507(2)	3621(6)	21(2)	
O(25)	1163(10)	7038(3)	1777(6)	28(2)	
O(26)	8514(9)	5784(2)	6356(6)	27(2)	
O(27)	6343(8)	8566(2)	7135(5)	14(1)	
O(28)	4316(8)	6821(2)	7723(5)	13(1)	
O(29)	1467(9)	8307(2)	4851(5)	19(1)	
O(30)	9474(9)	8636(2)	3102(6)	25(1)	
O(31)	4027(9)	6544(2)	2761(6)	26(2)	
O(32)	7849(9)	4160(2)	3485(6)	26(2)	
O(33)	6200(9)	4179(2)	7605(7)	33(2)	
O(34)	3112(7)	8841(2)	3325(4)	14(1)	
O(35)	3766(9)	9760(2)	2873(5)	24(1)	
O(36)	772(10)	9267(2)	4587(5)	26(1)	
O(37)	9338(9)	64(2)	5326(6)	25(2)	
O(38)	8346(11)	5516(3)	1033(6)	47(2)	
O(39)	636(12)	5939(2)	4748(6)	38(2)	
O(40)	8320(10)	9203(2)	8430(6)	30(2)	
O(41)	2029(10)	9597(3)	6537(6)	39(2)	
O(42)	1689(9)	5012(2)	9656(6)	27(2)	
O(43)	2952(10)	5646(2)	3349(5)	34(2)	
O(44)	7639(10)	7737(2)	6260(6)	24(1)	
O(45)	1606(9)	6318(2)	6663(6)	27(2)	

containing exclusively tertiary (Q^3) tetrahedra is rather an exception among the large number of structurally characterized oxosilicates. In the vast majority of cases, compounds with a Si:O ratio of 1:2.5 crystallize as single-layer, double-chain or double-ring silicates.⁴⁶ The fundamental structural units of the present framework are *dreier*

single chains running parallel [100], that is, the translation period along these chains is directly related to the *a* lattice parameter (see Figure 3A,B). Condensation of the chains along [010] results in the formation of layers parallel (001) which contain highly corrugated eight-membered rings. Finally, by sharing common oxygen corners a

TABLE 3 Bond lengths [Å] and bond angles [°] in $K_4CaSi_6O_{15}$. Distortion parameters for the tetrahedra and octahedra are given as well (λ : quadratic elongation; σ^2 : angle variance)

Ca(1)-O(20)	2.304(6)	Ca(1)-O(22)	2.332(7)	Ca(1)-O(44)	2.358(7)
Ca(1)-O(24)	2.386(7)	Ca(1)-O(29)	2.416(6)	Ca(1)-O(3)	2.491(6)
<Ca(1)-O>	2.381	λ	1.016	σ^2	55.18
Ca(2)-O(38)	2.280(7)	Ca(2)-O(5)	2.351(7)	Ca(2)-O(14)	2.385(7)
Ca(2)-O(32)	2.379(7)	Ca(2)-O(42)	2.423(7)	Ca(2)-O(1)	2.449(6)
<Ca(2)-O>	2.378	λ	1.017	σ^2	56.84
Ca(3)-O(40)	2.306(7)	Ca(3)-O(13)	2.310(6)	Ca(3)-O(16)	2.371(6)
Ca(3)-O(4)	2.396(6)	Ca(3)-O(18)	2.418(6)	Ca(3)-O(37)	2.426(6)
<Ca(3)-O>	2.371	λ	1.016	σ^2	53.67
K(1)-O(33)	2.694(6)	K(1)-O(3)	2.722(7)	K(1)-O(24)	2.750(7)
K(1)-O(39)	2.810(8)	K(1)-O(2)	2.921(6)	K(1)-O(25)	2.914(8)
K(1)-O(20)	3.007(7)	K(1)-O(31)	3.187(7)	K(1)-O(17)	3.275(8)
K(2)-O(29)	2.699(7)	K(2)-O(22)	2.959(7)	K(2)-O(19)	2.968(6)
K(2)-O(18)	2.976(6)	K(2)-O(41)	2.990(8)	K(2)-O(27)	3.028(6)
K(2)-O(4)	3.075(6)	K(2)-O(6)	3.097(8)		
K(3)-O(42)	2.611(8)	K(3)-O(14)	2.883(7)	K(3)-O(17)	2.921(8)
K(3)-O(43)	2.931(7)	K(3)-O(26)	3.026(6)	K(3)-O(11)	3.051(6)
K(3)-O(21)	3.070(6)	K(3)-O(38)	3.207(9)	K(3)-O(45)	3.237(7)
K(4)-O(15)	2.657(6)	K(4)-O(18)	2.713(6)	K(4)-O(12)	2.719(7)
K(4)-O(16)	2.734(6)	K(4)-O(34)	2.819(6)	K(4)-O(30)	2.891(7)
K(4)-O(13)	3.024(6)	K(4)-O(7)	3.204(6)	K(4)-O(25)	3.220(7)
K(51)-O(44)	2.716(13)	K(51)-O(34)	2.808(12)	K(51)-O(24)	2.812(14)
K(51)-O(29)	2.860(3)	K(51)-O(27)	3.131(16)	K(51)-O(7)	3.364(14)
K(52)-O(29)	2.561(8)	K(52)-O(44)	2.657(10)	K(52)-O(24)	2.689(9)
K(52)-O(22)	3.020(12)	K(52)-O(34)	3.079(11)	K(52)-O(20)	3.152(13)
K(52)-O(15)	3.306(11)				
K(61)-O(37)	2.546(18)	K(61)-O(4)	2.782(17)	K(61)-O(16)	2.816(12)
K(61)-O(23)	2.977(17)	K(61)-O(35)	3.320(2)	K(61)-O(40)	3.270(2)
K(61)-O(13)	3.320(3)				
K(62)-O(4)	2.690(3)	K(62)-O(37)	2.790(6)	K(62)-O(23)	2.870(3)
K(62)-O(35)	3.050(7)	K(62)-O(16)	2.880(3)		
K(71)-O(1)	2.592(9)	K(71)-O(5)	2.674(11)	K(71)-O(14)	2.711(12)
K(71)-O(32)	3.050(18)	K(71)-O(2)	3.157(17)	K(71)-O(28)	3.238(13)
K(71)-O(38)	3.220(2)				
K(72)-O(5)	2.730(16)	K(72)-O(14)	2.832(17)	K(72)-O(1)	2.89(4)
K(72)-O(2)	2.945(15)	K(72)-O(28)	3.035(18)	K(72)-O(31)	3.297(19)
K(8)-O(1)	2.689(7)	K(8)-O(32)	2.884(7)	K(8)-O(9)	2.904(7)
K(8)-O(28)	2.953(6)	K(8)-O(45)	3.038(8)	K(8)-O(3)	3.053(7)
K(8)-O(6)	3.198(7)	K(8)-O(44)	3.215(7)		
K(9)-O(3)	2.655(6)	K(9)-O(20)	2.676(7)	K(9)-O(22)	2.874(8)
K(9)-O(21)	3.064(7)	K(9)-O(28)	3.077(7)	K(9)-O(31)	3.144(8)
K(9)-O(45)	3.241(8)				
K(10)-O(18)	2.631(6)	K(10)-O(13)	2.728(7)	K(10)-O(8)	2.977(6)
K(10)-O(40)	3.040(7)	K(10)-O(4)	3.036(7)	K(10)-O(27)	3.073(6)
K(10)-O(16)	3.122(7)	K(10)-O(6)	3.194(8)	K(10)-O(7)	3.197(7)

(Continues)

TABLE 3 (Continued)

K(111)-O(38)	2.712(17)	K(111)-O(42)	2.85(4)	K(111)-O(32)	2.96(3)
K(111)-O(11)	3.006(17)	K(111)-O(43)	3.086(15)	K(111)-O(11)	3.20(3)
K(111)-O(17)	3.38(4)	K(111)-O(33)	3.45(3)		
K(112)-O(42)	2.619(11)	K(112)-O(38)	2.708(14)	K(112)-O(32)	2.825(11)
K(112)-O(5)	2.983(17)	K(112)-O(11)	3.13(2)	K(112)-O(14)	3.13(3)
K(112)-O(43)	3.28(2)				
K(12)-O(36)	2.721(7)	K(12)-O(10)	2.751(6)	K(12)-O(40)	2.805(7)
K(12)-O(37)	3.000(7)	K(12)-O(41)	3.150(8)	K(12)-O(23)	3.192(6)
K(12)-O(37)	3.207(7)	K(12)-O(35)	3.225(7)		
Si(1)-O(13)	1.557(6)	Si(1)-O(30)	1.622(7)	Si(1)-O(7)	1.630(6)
Si(1)-O(10)	1.631(6)				
<Si(1)-O>	1.610	λ	1.004	σ^2	15.05
Si(2)-O(38)	1.549(8)	Si(2)-O(33)	1.606(6)	Si(2)-O(17)	1.625(7)
Si(2)-O(11)	1.650(6)				
<Si(2)-O>	1.607	λ	1.003	σ^2	13.09
Si(3)-O(22)	1.560(7)	Si(3)-O(9)	1.622(6)	Si(3)-O(8)	1.637(6)
Si(3)-O(28)	1.646(6)				
<Si(3)-O>	1.616	λ	1.004	σ^2	16.22
Si(4)-O(20)	1.556(6)	Si(4)-O(25)	1.599(7)	Si(4)-O(15)	1.626(6)
Si(4)-O(31)	1.624(6)				
<Si(4)-O>	1.601	λ	1.003	σ^2	14.38
Si(5)-O(3)	1.556(6)	Si(5)-O(26)	1.628(6)	Si(5)-O(39)	1.618(7)
Si(5)-O(45)	1.625(7)				
<Si(5)-O>	1.607	λ	1.005	σ^2	20.31
Si(6)-O(42)	1.557(7)	Si(6)-O(39)	1.610(7)	Si(6)-O(17)	1.598(8)
Si(6)-O(43)	1.639(6)				
<Si(6)-O>	1.601	λ	1.006	σ^2	24.01
Si(7)-O(1)	1.555(6)	Si(7)-O(25)	1.620(7)	Si(7)-O(12)	1.620(6)
Si(7)-O(2)	1.637(6)				
<Si(7)-O>	1.608	λ	1.005	σ^2	23.74
Si(8)-O(4)	1.562(6)	Si(8)-O(41)	1.602(7)	Si(8)-O(35)	1.633(6)
Si(8)-O(23)	1.637(6)				
<Si(8)-O>	1.609	λ	1.006	σ^2	26.68
Si(9)-O(44)	1.550(7)	Si(9)-O(6)	1.620(7)	Si(9)-O(8)	1.639(6)
Si(9)-O(27)	1.658(6)				
<Si(9)-O>	1.617	λ	1.006	σ^2	26.31
Si(10)-O(32)	1.553(8)	Si(10)-O(11)	1.633(6)	Si(10)-O(21)	1.636(6)
Si(10)-O(26)	1.646(7)				
<Si(10)-O>	1.617	λ	1.006	σ^2	28.55
Si(11)-O(18)	1.568(6)	Si(11)-O(12)	1.621(6)	Si(11)-O(6)	1.619(7)
Si(11)-O(9)	1.642(6)				
<Si(11)-O>	1.612	λ	1.003	σ^2	10.53
Si(12)-O(16)	1.562(7)	Si(12)-O(35)	1.616(6)	Si(12)-O(34)	1.627(5)
Si(12)-O(10)	1.642(6)				
<Si(12)-O>	1.612	λ	1.005	σ^2	20.76
Si(13)-O(40)	1.556(7)	Si(13)-O(23)	1.637(5)	Si(13)-O(27)	1.638(6)

(Continues)

TABLE 3 (Continued)

Si(13)-O(19)	1.645(6)				
<Si(13)-O>	1.619	λ	1.004	σ^2	18.26
Si(14)-O(24)	1.566(7)	Si(14)-O(15)	1.633(6)	Si(14)-O(7)	1.638(6)
Si(14)-O(2)	1.641(6)				
<Si(14)-O>	1.620	λ	1.008	σ^2	32.38
Si(15)-O(29)	1.555(6)	Si(15)-O(30)	1.615(7)	Si(15)-O(36)	1.625(6)
Si(15)-O(34)	1.658(5)				
<Si(15)-O>	1.613	λ	1.005	σ^2	22.63
Si(16)-O(37)	1.565(6)	Si(16)-O(19)	1.623(6)	Si(16)-O(41)	1.621(7)
Si(16)-O(36)	1.624(6)				
<Si(16)-O>	1.608	λ	1.006	σ^2	23.89
Si(17)-O(14)	1.558(7)	Si(17)-O(43)	1.599(6)	Si(17)-O(31)	1.632(6)
Si(17)-O(33)	1.637(6)				
<Si(17)-O>	1.607	λ	1.010	σ^2	41.21
Si(18)-O(5)	1.550(7)	Si(18)-O(45)	1.606(7)	Si(18)-O(28)	1.640(6)
Si(18)-O(21)	1.648(6)				
<Si(18)-O>	1.611	λ	1.007	σ^2	32.74
O-Si-O angles					
O(13)-Si(1)-O(30)	113.1(4)	O(13)-Si(1)-O(7)	111.3(3)	O(30)-Si(1)-O(7)	107.3(3)
O(13)-Si(1)-O(10)	112.8(3)	O(30)-Si(1)-O(10)	103.0(3)	O(7)-Si(1)-O(10)	108.8(3)
O(38)-Si(2)-O(33)	113.6(5)	O(38)-Si(2)-O(17)	112.2(4)	O(33)-Si(2)-O(17)	104.8(4)
O(38)-Si(2)-O(11)	111.7(4)	O(33)-Si(2)-O(11)	106.5(3)	O(33)-Si(2)-O(11)	106.5(3)
O(22)-Si(3)-O(9)	113.3(4)	O(22)-Si(3)-O(8)	112.1(3)	O(9)-Si(3)-O(8)	106.1(3)
O(22)-Si(3)-O(28)	113.6(3)	O(9)-Si(3)-O(28)	106.3(3)	O(8)-Si(3)-O(28)	104.6(3)
O(20)-Si(4)-O(25)	112.8(4)	O(20)-Si(4)-O(15)	113.8(4)	O(25)-Si(4)-O(15)	103.9(4)
O(20)-Si(4)-O(31)	110.6(4)	O(25)-Si(4)-O(31)	109.2(4)	O(15)-Si(4)-O(31)	106.3(3)
O(3)-Si(5)-O(26)	116.8(3)	O(3)-Si(5)-O(39)	111.2(4)	O(26)-Si(5)-O(39)	104.4(3)
O(3)-Si(5)-O(45)	110.7(4)	O(26)-Si(5)-O(45)	106.1(4)	O(39)-Si(5)-O(45)	106.9(4)
O(42)-Si(6)-O(39)	117.4(4)	O(42)-Si(6)-O(17)	111.7(4)	O(39)-Si(6)-O(17)	109.1(4)
O(42)-Si(6)-O(43)	108.6(4)	O(39)-Si(6)-O(43)	103.4(4)	O(17)-Si(6)-O(43)	105.6(4)
O(1)-Si(7)-O(25)	113.3(4)	O(1)-Si(7)-O(12)	114.4(4)	O(25)-Si(7)-O(12)	107.3(4)
O(1)-Si(7)-O(2)	113.0(3)	O(25)-Si(7)-O(2)	104.6(4)	O(12)-Si(7)-O(2)	103.2(3)
O(4)-Si(8)-O(41)	114.5(4)	O(4)-Si(8)-O(35)	109.5(3)	O(41)-Si(8)-O(35)	109.2(4)
O(4)-Si(8)-O(23)	115.4(3)	O(41)-Si(8)-O(23)	101.6(4)	O(35)-Si(8)-O(23)	106.2(3)
O(44)-Si(9)-O(6)	113.1(4)	O(44)-Si(9)-O(8)	114.5(3)	O(6)-Si(9)-O(8)	103.5(4)
O(44)-Si(9)-O(27)	113.7(4)	O(6)-Si(9)-O(27)	107.5(3)	O(8)-Si(9)-O(27)	103.5(3)
O(32)-Si(10)-O(11)	114.8(4)	O(32)-Si(10)-O(21)	113.9(3)	O(11)-Si(10)-O(21)	103.2(3)
O(32)-Si(10)-O(26)	113.6(4)	O(11)-Si(10)-O(26)	104.5(3)	O(21)-Si(10)-O(26)	105.8(3)
O(18)-Si(11)-O(12)	112.2(4)	O(18)-Si(11)-O(6)	110.4(3)	O(12)-Si(11)-O(6)	108.1(4)
O(18)-Si(11)-O(9)	113.7(3)	O(12)-Si(11)-O(9)	105.5(3)	O(6)-Si(11)-O(9)	106.6(4)
O(16)-Si(12)-O(35)	113.7(3)	O(16)-Si(12)-O(34)	114.3(3)	O(35)-Si(12)-O(34)	107.8(3)
O(16)-Si(12)-O(10)	111.7(3)	O(35)-Si(12)-O(10)	104.6(3)	O(34)-Si(12)-O(10)	103.9(3)
O(40)-Si(13)-O(23)	110.8(3)	O(40)-Si(13)-O(27)	113.4(3)	O(23)-Si(13)-O(27)	108.1(3)
O(40)-Si(13)-O(19)	114.4(4)	O(23)-Si(13)-O(19)	103.5(3)	O(27)-Si(13)-O(19)	105.9(3)
O(24)-Si(14)-O(15)	111.9(4)	O(24)-Si(14)-O(7)	114.5(4)	O(15)-Si(14)-O(7)	101.2(3)
O(24)-Si(14)-O(2)	114.4(3)	O(15)-Si(14)-O(2)	103.3(3)	O(7)-Si(14)-O(2)	110.2(3)

(Continues)

TABLE 3 (Continued)

O(29)-Si(15)-O(30)	111.9(4)	O(29)-Si(15)-O(36)	115.2(3)	O(30)-Si(15)-O(36)	107.9(4)
O(29)-Si(15)-O(34)	113.0(3)	O(30)-Si(15)-O(34)	104.0(3)	O(36)-Si(15)-O(34)	104.0(3)
O(37)-Si(16)-O(19)	117.9(3)	O(37)-Si(16)-O(41)	111.6(4)	O(19)-Si(16)-O(41)	104.9(4)
O(37)-Si(16)-O(36)	108.2(3)	O(19)-Si(16)-O(36)	104.8(3)	O(41)-Si(16)-O(36)	109.0(4)
O(14)-Si(17)-O(43)	112.6(4)	O(14)-Si(17)-O(31)	115.4(4)	O(43)-Si(17)-O(31)	111.9(4)
O(14)-Si(17)-O(33)	113.2(4)	O(43)-Si(17)-O(33)	102.7(4)	O(31)-Si(17)-O(33)	99.7(3)
O(5)-Si(18)-O(45)	115.0(4)	O(5)-Si(18)-O(28)	113.6(4)	O(45)-Si(18)-O(28)	106.7(3)
O(5)-Si(18)-O(21)	114.4(4)	O(45)-Si(18)-O(21)	102.9(4)	O(28)-Si(18)-O(21)	103.1(3)
Si-O-Si angles					
Si(7)-O(2)-Si(14)	147.1(4)	Si(11)-O(6)-Si(9)	165.7(5)	Si(14)-O(7)-Si(1)	145.2(4)
Si(9)-O(8)-Si(3)	137.0(4)	Si(3)-O(9)-Si(11)	142.3(4)	Si(1)-O(10)-Si(12)	133.5(4)
Si(10)-O(11)-Si(2)	135.4(4)	Si(11)-O(12)-Si(7)	149.0(5)	Si(4)-O(15)-Si(14)	139.0(4)
Si(2)-O(17)-Si(6)	168.2(5)	Si(16)-O(19)-Si(13)	143.9(4)	Si(10)-O(21)-Si(18)	133.6(4)
Si(13)-O(23)-Si(8)	134.7(4)	Si(4)-O(25)-Si(7)	171.0(5)	Si(5)-O(26)-Si(10)	142.9(4)
Si(13)-O(27)-Si(9)	136.3(4)	Si(3)-O(28)-Si(18)	134.5(4)	Si(1)-O(30)-Si(15)	164.5(5)
Si(17)-O(31)-Si(4)	144.7(4)	Si(2)-O(33)-Si(17)	137.5(4)	Si(12)-O(34)-Si(15)	143.8(4)
Si(12)-O(35)-Si(8)	147.2(4)	Si(15)-O(36)-Si(16)	146.0(4)	Si(6)-O(39)-Si(5)	153.3(4)
Si(8)-O(41)-Si(16)	169.1(6)	Si(17)-O(43)-Si(6)	152.8(5)	Si(18)-O(45)-Si(5)	164.5(5)
O-Ca-O angles					
O(20)-Ca(1)-O(22)	86.9(3)	O(20)-Ca(1)-O(44)	170.8(3)	O(22)-Ca(1)-O(44)	96.5(3)
O(20)-Ca(1)-O(24)	89.0(2)	O(22)-Ca(1)-O(24)	175.9(3)	O(44)-Ca(1)-O(24)	87.5(2)
O(20)-Ca(1)-O(29)	90.9(2)	O(22)-Ca(1)-O(29)	77.8(2)	O(44)-Ca(1)-O(29)	98.2(2)
O(24)-Ca(1)-O(29)	102.1(2)	O(20)-Ca(1)-O(3)	90.4(2)	O(22)-Ca(1)-O(3)	97.1(2)
O(44)-Ca(1)-O(3)	80.7(2)	O(24)-Ca(1)-O(3)	83.1(2)	O(29)-Ca(1)-O(3)	174.7(2)
O(38)-Ca(2)-O(5)	170.8(3)	O(38)-Ca(2)-O(14)	92.2(3)	O(5)-Ca(2)-O(14)	84.7(2)
O(38)-Ca(2)-O(32)	87.8(3)	O(5)-Ca(2)-O(32)	95.6(3)	O(14)-Ca(2)-O(32)	178.0(3)
O(38)-Ca(2)-O(42)	87.6(3)	O(5)-Ca(2)-O(42)	83.3(3)	O(14)-Ca(2)-O(42)	80.8(2)
O(32)-Ca(2)-O(42)	101.2(2)	O(38)-Ca(2)-O(1)	91.1(3)	O(5)-Ca(2)-O(1)	98.0(2)
O(14)-Ca(2)-O(1)	99.7(2)	O(32)-Ca(2)-O(1)	78.3(2)	O(42)-Ca(2)-O(1)	178.6(3)
O(40)-Ca(3)-O(13)	91.2(2)	O(40)-Ca(3)-O(16)	178.0(3)	O(13)-Ca(3)-O(16)	90.7(2)
O(40)-Ca(3)-O(4)	91.1(2)	O(13)-Ca(3)-O(4)	171.0(2)	O(16)-Ca(3)-O(4)	87.0(2)
O(40)-Ca(3)-O(18)	97.1(2)	O(13)-Ca(3)-O(18)	91.4(2)	O(16)-Ca(3)-O(18)	83.2(2)
O(4)-Ca(3)-O(18)	79.7(2)	O(40)-Ca(3)-O(37)	82.1(2)	O(13)-Ca(3)-O(37)	84.2(2)
O(16)-Ca(3)-O(37)	97.8(2)	O(4)-Ca(3)-O(37)	104.7(2)	O(18)-Ca(3)-O(37)	175.4(2)

three-dimensional framework is formed, where the stacking of neighboring tetrahedral sheets is parallel to [001] (see Figure 4).

Concerning the individual Si–O bond lengths, two groups can be distinguished: distances between Si and the non-bridging oxygen atoms are significantly shorter (1.549–1.568 Å) than the Si–O_{br} distances (1.598–1.658 Å). This type of shortening is well-known for silicates and can be attributed to the stronger attraction between oxygen and silicon than between oxygen and calcium/potassium. While the mean values of the O–Si–O angles for the tetrahedra are close to the ideal value of 109.47°, individual O–Si–O angles range from 99.7° to 117.9°, indicating

that the tetrahedra deviate considerably from regularity. However, the scatter is similar to the values reported in the literature for other interrupted silicate frameworks such as γ -Na₂Si₂O₅⁴⁷ or K₈CaSi₁₀O₂₅.² The Si–O–Si angles exhibit a spread between 133.5° and 171.0° with an average value of 147.5°. This mean value is 7.5° higher than the value of 140° reported for an unstrained Si–O–Si angle⁴⁶ and almost identical to the value observed in K₈CaSi₁₀O₂₅. Bond valence sums (BVS) for the Si atoms are close to the expected value of 4 (see Table 2).

Charge compensation within the structure is achieved by the incorporation of Ca- and K-cations. The Ca-ions are coordinated by six oxygen ligands forming [CaO₆]-octahedra

TABLE 4 Anisotropic displacement parameters ($\text{\AA}^2 \times 10^3$) for $\text{K}_4\text{CaSi}_6\text{O}_{15}$. The anisotropic displacement factor exponent takes the form: $-2\pi^2[h^2a^{*2}U_{11} + \dots + 2hka^*b^*U_{12}]$

	U_{11}	U_{22}	U_{33}	U_{23}	U_{13}	U_{12}
Ca(1)	7(1)	11(1)	6(1)	1(1)	0(1)	0(1)
Ca(2)	11(1)	8(1)	11(1)	0(1)	-2(1)	-1(1)
Ca(3)	12(1)	9(1)	8(1)	0(1)	-1(1)	-1(1)
K(1)	22(1)	13(1)	15(1)	3(1)	-1(1)	-4(1)
K(2)	29(1)	15(1)	18(1)	5(1)	3(1)	1(1)
K(3)	22(1)	17(1)	28(1)	-7(1)	3(1)	-1(1)
K(4)	26(1)	12(1)	15(1)	-1(1)	-5(1)	2(1)
K(51)	70(12)	103(16)	20(4)	-1(6)	-7(5)	70(13)
K(52)	17(2)	52(5)	22(2)	0(2)	1(2)	14(2)
K(61)	23(5)	54(6)	23(3)	4(3)	-4(3)	-25(3)
K(62)	52(13)	99(15)	21(6)	-17(8)	-8(7)	-28(14)
K(71)	23(3)	61(7)	27(3)	7(3)	0(2)	-21(4)
K(72)	60(14)	82(17)	30(4)	7(6)	-4(5)	-58(13)
K(8)	21(1)	17(1)	21(1)	-6(1)	2(1)	-4(1)
K(9)	33(1)	143(3)	20(1)	17(2)	8(1)	50(2)
K(10)	19(1)	54(1)	19(1)	-7(1)	1(1)	-8(1)
K(111)	42(10)	78(16)	26(4)	-20(6)	8(6)	-36(11)
K(112)	20(3)	50(6)	23(3)	10(3)	-2(2)	-4(3)
K(12)	39(1)	15(1)	36(1)	-7(1)	-5(1)	1(1)
Si(1)	10(1)	9(1)	10(1)	1(1)	-2(1)	-1(1)
Si(2)	11(1)	6(1)	13(1)	-1(1)	-4(1)	2(1)
Si(3)	7(1)	7(1)	12(1)	1(1)	1(1)	0(1)
Si(4)	6(1)	8(1)	8(1)	0(1)	1(1)	0(1)
Si(5)	11(1)	7(1)	8(1)	1(1)	0(1)	1(1)
Si(6)	11(1)	7(1)	9(1)	-1(1)	0(1)	0(1)
Si(7)	10(1)	6(1)	6(1)	0(1)	0(1)	-1(1)
Si(8)	14(1)	7(1)	12(1)	1(1)	-3(1)	-1(1)
Si(9)	5(1)	9(1)	9(1)	-1(1)	1(1)	-2(1)
Si(10)	10(1)	6(1)	16(1)	-1(1)	-4(1)	1(1)
Si(11)	7(1)	7(1)	8(1)	2(1)	1(1)	0(1)
Si(12)	14(1)	8(1)	11(1)	1(1)	-1(1)	0(1)
Si(13)	12(1)	7(1)	11(1)	0(1)	-3(1)	1(1)
Si(14)	7(1)	10(1)	10(1)	3(1)	1(1)	0(1)
Si(15)	12(1)	8(1)	9(1)	1(1)	-2(1)	-1(1)
Si(16)	15(1)	7(1)	10(1)	2(1)	-3(1)	-2(1)
Si(17)	10(1)	7(1)	12(1)	0(1)	-1(1)	-3(1)
Si(18)	13(1)	7(1)	13(1)	-2(1)	0(1)	1(1)
O(1)	30(3)	8(3)	14(3)	-6(2)	0(3)	0(2)
O(2)	17(3)	19(3)	17(3)	1(2)	2(2)	-5(2)
O(3)	18(3)	8(3)	20(3)	2(2)	-4(2)	2(2)
O(4)	23(3)	22(3)	18(3)	5(2)	4(2)	-4(2)
O(5)	28(3)	40(4)	24(4)	6(3)	6(3)	-13(3)
O(6)	17(3)	27(4)	32(4)	-4(3)	-16(3)	0(3)

(Continues)

TABLE 4 (Continued)

	U_{11}	U_{22}	U_{33}	U_{23}	U_{13}	U_{12}
O(7)	17(3)	6(3)	26(3)	2(2)	-2(2)	-2(2)
O(8)	18(3)	18(3)	13(3)	-6(2)	7(2)	-11(2)
O(9)	16(3)	15(3)	32(4)	-5(3)	14(3)	0(2)
O(10)	13(3)	12(3)	28(3)	-7(2)	0(2)	1(2)
O(11)	12(3)	9(3)	32(4)	-2(3)	4(3)	-2(2)
O(12)	32(3)	19(3)	21(3)	4(3)	16(3)	-4(3)
O(13)	23(3)	29(3)	18(3)	5(3)	8(3)	-6(3)
O(14)	27(3)	19(3)	17(3)	-4(3)	-13(3)	-4(3)
O(15)	6(3)	20(3)	35(4)	14(3)	3(3)	0(2)
O(16)	24(3)	21(3)	15(3)	3(2)	-8(3)	-5(2)
O(17)	22(3)	40(4)	37(4)	-4(4)	-22(3)	-4(3)
O(18)	12(3)	10(3)	15(3)	0(2)	1(2)	-1(2)
O(19)	20(3)	14(3)	35(4)	4(2)	14(3)	-2(2)
O(20)	27(3)	36(4)	11(3)	3(3)	10(3)	10(3)
O(21)	24(3)	20(3)	19(3)	-11(2)	-8(2)	14(2)
O(22)	29(4)	21(3)	19(4)	5(3)	-14(3)	0(3)
O(23)	22(3)	20(3)	26(3)	8(2)	9(2)	11(2)
O(24)	24(3)	24(3)	13(4)	-1(3)	-3(3)	4(3)
O(25)	20(3)	37(4)	26(4)	1(3)	-12(3)	3(3)
O(26)	31(3)	16(3)	36(4)	9(3)	11(3)	-1(2)
O(27)	11(3)	12(3)	20(3)	2(2)	0(2)	-1(2)
O(28)	13(3)	6(3)	19(3)	-1(2)	-3(2)	3(2)
O(29)	21(3)	16(3)	19(3)	6(2)	-3(3)	-3(2)
O(30)	18(3)	32(3)	24(3)	4(3)	-12(3)	2(3)
O(31)	25(3)	12(3)	39(4)	-13(3)	-10(3)	10(3)
O(32)	26(3)	22(4)	28(4)	7(3)	-11(3)	1(3)
O(33)	18(3)	15(3)	64(5)	19(3)	-12(3)	-7(2)
O(34)	15(3)	13(3)	15(3)	1(2)	10(2)	-3(2)
O(35)	43(4)	8(3)	22(3)	3(2)	10(3)	4(3)
O(36)	53(4)	9(3)	19(3)	-3(2)	18(3)	-3(3)
O(37)	27(3)	9(3)	39(4)	7(3)	2(3)	5(2)
O(38)	50(5)	63(5)	28(4)	8(4)	10(4)	-34(4)
O(39)	66(5)	18(3)	31(4)	-9(3)	22(3)	10(3)
O(40)	43(4)	22(3)	22(3)	1(3)	-18(3)	-4(3)
O(41)	32(4)	51(5)	30(4)	11(3)	-20(3)	-15(3)
O(42)	29(3)	13(3)	37(4)	-5(3)	-16(3)	1(3)
O(43)	39(4)	40(4)	27(4)	4(3)	19(3)	-22(3)
O(44)	31(3)	22(3)	19(4)	-6(3)	11(3)	5(3)
O(45)	19(3)	19(3)	40(4)	-3(3)	-18(3)	2(2)

showing only minor distortions and almost ideal BVS values (see Table 2). Each of the three octahedra in the asymmetric unit shares all corners with neighboring tetrahedra. Indeed, the structure could be also described as a mixed tetrahedral-octahedral network in which the K-ions occupy the extra-framework sites (see Figure 5A,B). Initially, structure

solution indicated the presence of twelve fully occupied potassium positions. However, the refinement of the anisotropic temperature displacement parameters showed that at least four potassium sites are more adequately modeled as a split position with K-K distances between 0.401 and 0.794 Å. Notably, the split K-positions occur exclusively at $x \approx \frac{1}{2}$ in

the channel-like structures of the mixed polyhedral framework running along [010]. Split positions and partially occupied sites are not uncommon for extra-framework cations and have been observed in many framework silicates such as zeolite-type structures.⁴⁸ The remaining potassium ions are located in slabs parallel (100) formed by corner-sharing octahedra and tetrahedra which are centered at $x \approx 0$. In general, the potassium atoms in $K_4CaSi_6O_{15}$ show irregular

coordination environments with five to nine next oxygen neighbors (see Table 3). Some of the corresponding bond valance sums are low. This “underbonding” indicates that the K atoms in the tunnels are too small and do not fit so well into the voids between the surrounding $[SiO_4]$ - and $[CaO_6]$ -units of the framework.

3.3 | Topological aspects

The SiO_4 -tetrahedra in $K_4CaSi_6O_{15}$ are linked into a 3-dimensional 3-connected net with a framework density of $15.6 \text{ T-atoms}/1000 \text{ \AA}^3$. In order to characterize this network in more detail, a topological analysis has been performed using the program ToposPro.⁴⁹ For this purpose, the crystal structure has been described by a graph composed of the vertices (sites of the Si-cations as well as O anions) and edges (bonds) between them. The nodes of the graph can be classified according to their *coordination sequences* $\{N_k\}$. This number sequence represents a set of integers $\{N_k\}$ ($k = 1, \dots, n$), where N_k is the number of sites in the k th coordination sphere of the respective atom that has been selected to be the central one.⁵⁰ The corresponding values for the relevant symmetrically independent Si-sites up to $n = 10$ (without the oxygen nodes), as well as the cumulative numbers Cum_{10} including the central atoms, are listed in Table 5. Supplementary, the *extended point symbols* listing all shortest circuits for each angle for any non-equivalent Si-atom have been determined. On the basis of the coordination sequences, two types of Si-sites can be distinguished. Furthermore, all nodes have the

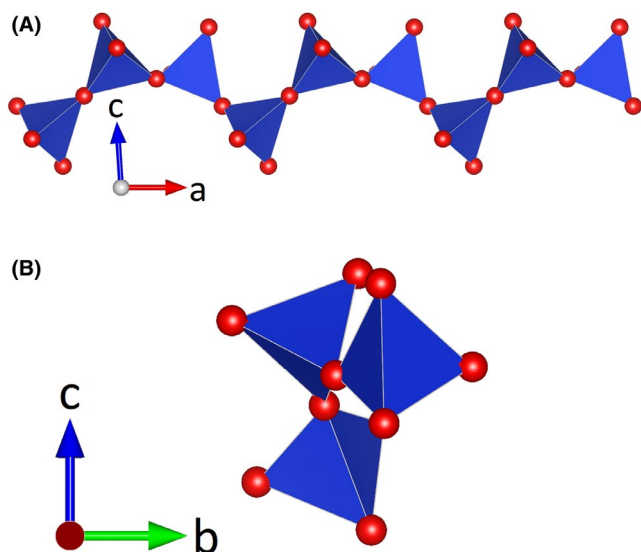


FIGURE 3 Projections of one of the fundamental *dreier* single chains of the tetrahedral network (A) perpendicular and (B) parallel to the chain direction. Oxygen atoms are given as red spheres. (Color online)

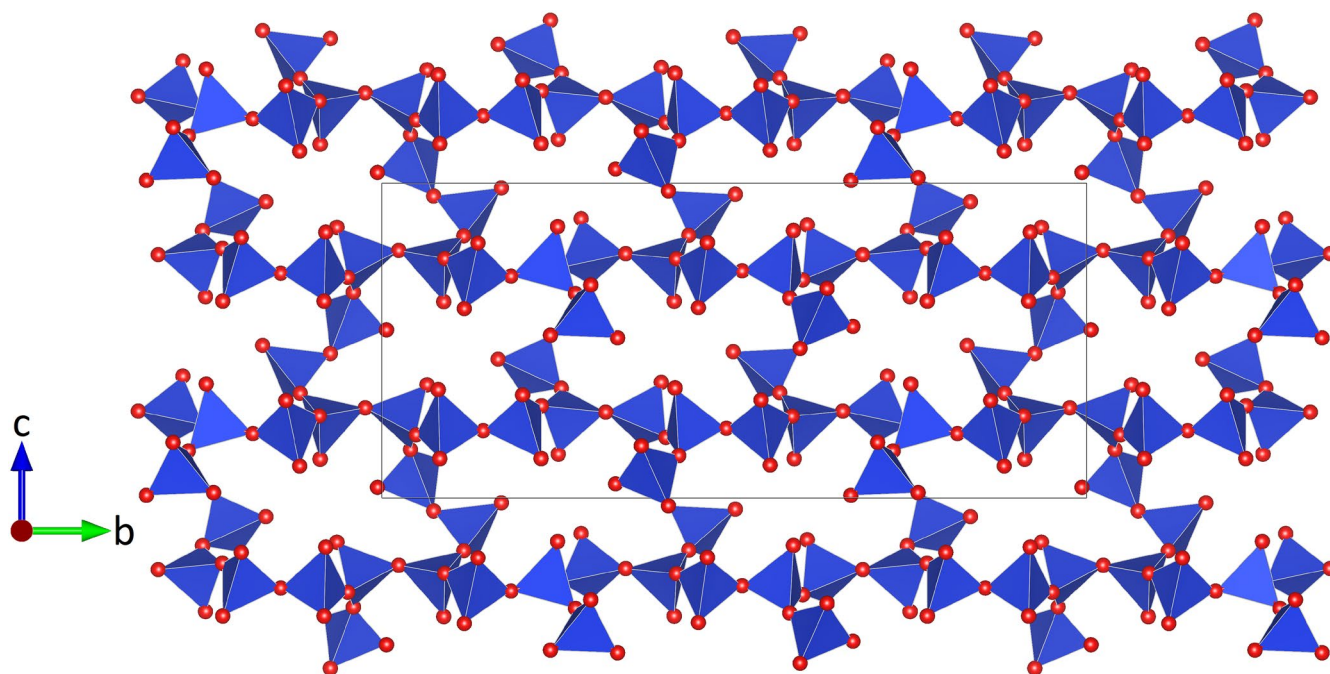


FIGURE 4 Projection of the tetrahedral framework along [100]

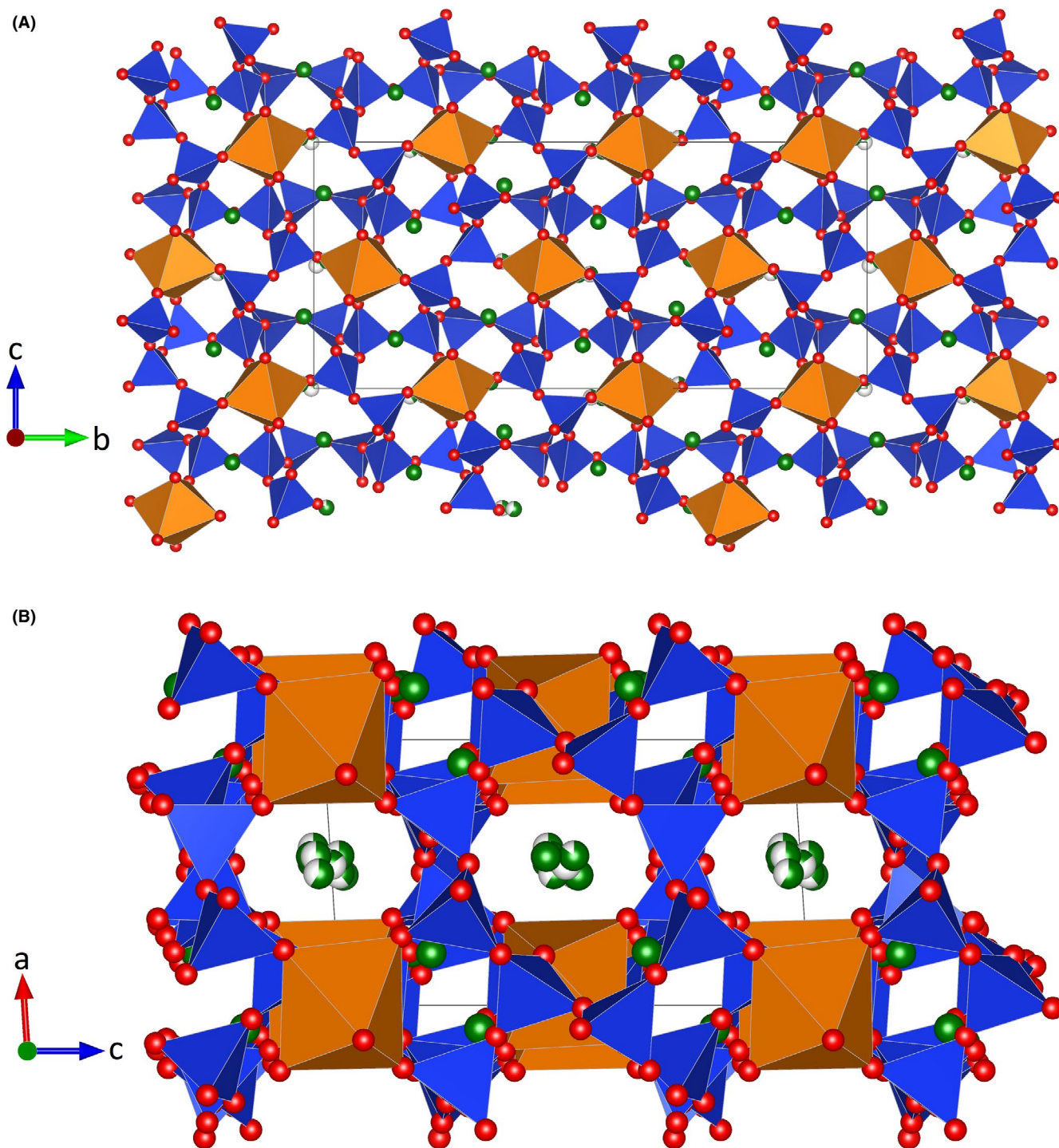


FIGURE 5 Projections of the whole crystal structure of $K_4CaSi_6O_{15}$ parallel to (A) [100] and (B) [010], respectively. $[CaO_6]$ -octahedra are shown in orange. Green spheres represent the potassium cations. White sectors within the spheres indicate partial occupancy of the split positions

same extended point symbols (see Figure 6). The topological density, TD_{10} , representing the rounded average of the Cum_{10} values for all central atoms in the asymmetric unit has a value of 504. The derived topological parameters allowed for a classification of the network using the Reticular Chemistry Structure Resource (RCSR) database.⁵¹ Notably,

the tetrahedral net observed in the present compound corresponds to the already existing entry *eth* of this collection of crystal nets. To the best of our knowledge, $K_4CaSi_6O_{15}$ is the first inorganic representative for this net type that has been previously observed in metal–organic frameworks or molecular structures only.

TABLE 5 Coordination sequences $\{N_k\}$ of the tetrahedrally coordinated nodes (without the oxygen atoms), as well as the extended point symbols for the framework of $K_4CaSi_6O_{15}$. Vertex-type 1: Si1, Si2, Si3, Si4, Si8, Si9, Si10, Si12, Si13, Si14, Si17, Si18; Vertex-type 2: Si5, Si6, Si7, Si11, Si15, Si16. Cum₁₀: cumulative numbers of the coordination sequence including the central atom

Vertex	Coordination sequences $\{N_k\}$ ($k=1-10$)										Cum ₁₀	Extended point symbols
	1	2	3	4	5	6	7	8	9	10		
1	3	6	12	20	32	48	63	81	105	132	503	8.8.8 ₂
2	3	6	12	20	32	48	65	84	105	130	506	8.8.8 ₂

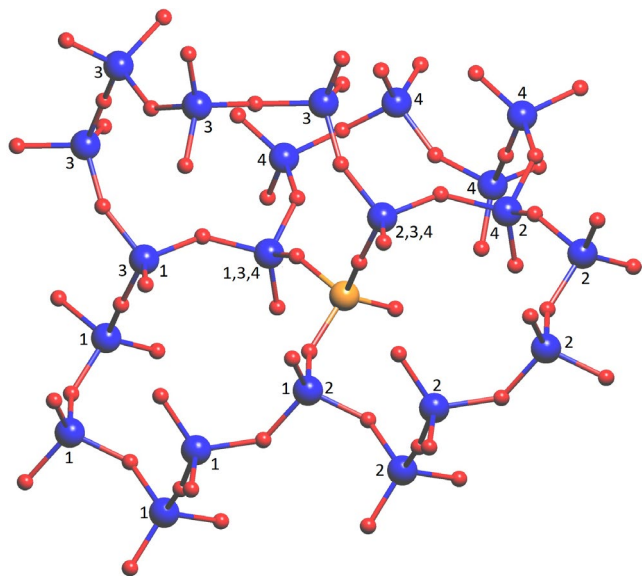


FIGURE 6 Graphical representation of the extended point symbol 8.8.8₂ observed for one selected reference atom (Si18, shown in yellow). For easier identification of the individual circuits, numbers from 1 to 4 indicate to which of the eight-membered rings each tetrahedron belongs

4 | DISCUSSION

Our investigations confirm the existence of $K_4CaSi_6O_{15}$ which was first mentioned in 1930. Furthermore, its congruent melting behavior could be validated (T_m : 956°C (our data) and 959°C (Morey et al.¹)). Hitherto, two other phases of the ternary system K_2O – CaO – SiO_2 have been verified with their compositions plotting along a line with constant silica content of 66.7 mol%: $K_8CaSi_{10}O_{25}$ (or $K_{9.6}Ca_{1.2}Si_{12}O_{30}$)² and $K_2CaSi_4O_{10}$,⁸ respectively. When normalized to five oxygen atoms *p.f.u.*, all possible compositions can be conveniently expressed using the following general formula: $K_{2-2x}Ca_xSi_2O_5$. Following this concept, the two aforementioned phases could be formulated as $K_{1.60}Ca_{0.20}Si_2O_5$ and $K_{1.00}Ca_{0.50}Si_2O_5$, respectively. $K_4CaSi_6O_{15}$ (or $K_{1.33}Ca_{0.33}Si_2O_5$) lies just in between these two phases.

It is noteworthy, that the two potassium-richest compounds both belong to the group of interrupted framework silicates. Though they are structurally not related and are characterized by different topological features, the calcium

ions in both compounds are octahedrally coordinated and each $[CaO_6]$ -polyhedron shares all six corners with adjacent $[SiO_4]$ -tetrahedra. The potassium cations located in the tunnel-like cavities of both networks exhibit split positions.

With decreasing K-concentration, a principally new connectivity of the silicate anions occurs. In fact, $K_2CaSi_4O_{10}$ ($K_{1.00}Ca_{0.50}Si_2O_5$) belongs to the group tubular chain silicates containing loop-branched *dreier* double chains. The coordination number of the calcium atoms is reduced from six to five. Each two of the Ca-centered trigonal bipyramids share a common edge forming $[Ca_2O_8]$ -moieties.

For now, it is unclear if other crystalline phases with higher Ca-contents exist along the tie line $K_2Si_2O_5$ ($x = 0$) – $CaSi_2O_5$ ($x = 1$). At ambient pressure, $CaSi_2O_5$ is not a stable compound in the binary phase diagram CaO – SiO_2 ,⁵² but this phase has been successfully synthesized at 11 GPa and 1350°C.⁵³ In their contribution from 1930, Morey et al.¹ mentioned the preparation of $K_2Ca_2Si_6O_{15}$ ($x = 0.67$). However, in a corrigendum published only 1 year later, a modified composition ($K_2Ca_3Si_6O_{16}$) with a different silica content (60 mol%) was suggested for this compound.⁵⁴ Interestingly, in the related Na_2O – CaO – SiO_2 system $Na_2Ca_3Si_6O_{16}$ or devitrite has been described.⁵⁵ However, from a structural point of view, it is questionable whether the hypothetical K- and the Na-compound would be isotypic. A unique feature of the devitrite structure is the presence of quadruple silicate chains showing a very strong corrugation in order to satisfy the bonding requirements of the interstitial sodium cations. Given that the ionic radius of K^+ is considerably larger than the radius of Na^+ , it is likely that $K_2Ca_3Si_6O_{16}$ would adapt a different structure type.

Moreover, the compositions of postulated $K_2Ca_3Si_6O_{16}$ and structurally characterized $K_2Ca_4Si_8O_{21}$ (7.7 mol% K_2O , 30.8 mol% CaO , and 61.5 mol% SiO_2)⁵⁶ are very close to each other. Therefore, it cannot be excluded that $K_2Ca_3Si_6O_{16}$ is misinterpreted $K_2Ca_4Si_8O_{21}$. Further experimental studies are definitely necessary to settle the question if $K_{2-2x}Ca_xSi_2O_5$ -compounds with $x > 0.50$ do exist or not.

5 | CONCLUSIONS

The results of our investigation on $K_4CaSi_6O_{15}$ represent another piece of the mosaic for a better understanding of the ternary

system $\text{K}_2\text{O}-\text{CaO}-\text{SiO}_2$. The proof of its existence and the possibility to obtain $\text{K}_4\text{CaSi}_6\text{O}_{15}$ in phase-pure form and larger quantities will allow for the determination of other physico-chemical properties. A key parameter with respect to thermochemical behavior is the molar heat capacity C_p . Knowledge of C_p -data of the ternary phase over a wide range of temperatures will enable the modeling of the contribution of this compound to the phase diagram using computational techniques. Determination of this property for $\text{K}_4\text{CaSi}_6\text{O}_{15}$ is planned in due course.


With a total of currently nine structurally characterized crystalline compounds at ambient pressure, the system $\text{K}_2\text{O}-\text{CaO}-\text{SiO}_2$ belongs to the most complex ternary silicate systems. Moreover, it cannot be excluded that there are still other phases to be discovered. For this purpose, systematic in-situ high-temperature diffraction studies would be of great interest for the detection of novel stable or metastable compounds, as well as to decipher the reaction pathways leading to their formation. Ninety years after its first comprehensive description, the $\text{K}_2\text{O}-\text{CaO}-\text{SiO}_2$ phase diagram may still hold surprises and offers a plethora of research activities.

ACKNOWLEDGMENT

This research was funded in part by the Austrian Science Fund (FWF), Grant no. P 30754. For open access, the corresponding author has applied a CC BY public license copyright license to any Author Accepted Manuscript version arising from this submission.

ORCID

Hang Liu  <https://orcid.org/0000-0003-0128-1265>

Volker Kahlenberg  <https://orcid.org/0000-0002-0652-7984>

Hannes Krüger  <https://orcid.org/0000-0002-7652-1166>

Herwig Schottenberger  <https://orcid.org/0000-0002-5212-9020>

REFERENCES

- Morey GW, Kracek FC, Bowen NL. The ternary system $\text{K}_2\text{O}-\text{CaO}-\text{SiO}_2$. *J Soc Glass Technol*. 1930;14:149–87.
- Kahlenberg V, Kaindl R, Többs DM. The crystal structure of the interrupted framework silicate $\text{K}_{9.6}\text{Ca}_{1.2}\text{Si}_{12}\text{O}_{30}$ determined from laboratory X-ray diffraction data. *J Solid State Chem*. 2006;179:1948–56.
- Arroyabe E, Kaindl R, Kahlenberg V. Structural and Raman spectroscopic investigations of $\text{K}_4\text{BaSi}_3\text{O}_9$ and $\text{K}_4\text{CaSi}_3\text{O}_9$. *Z Anorg Allg Chem*. 2009;635:337–45.
- Schmidmair D, Kahlenberg V, Praxmarer A, Perfler L, Mair P. Investigations on the crystal-structure and non-ambient behaviour of $\text{K}_2\text{Ca}_2\text{Si}_8\text{O}_{19}$ - a new potassium calcium silicate. *J Solid State Chem*. 2017;253:336–46.
- Arroyabe E, Kahlenberg V. Structural investigations on the fertilizer component $\text{K}_2\text{Ca}_2\text{Si}_2\text{O}_7$. *Eur J Miner*. 2011;23:101–10.
- Schmidmair D, Kahlenberg V, Perfler L, Tribus M, Hildebrandt J, Többs DM. On the ambient pressure polymorph of $\text{K}_2\text{Ca}_3\text{Si}_3\text{O}_{10}$ - an unusual mixed-anion silicate and its structural and spectroscopic characterization. *J Solid State Chem*. 2015;228:90–8.
- Arroyabe E, Kaindl R, Többs DM, Kahlenberg V. $\text{K}_2\text{Ca}_6\text{Si}_4\text{O}_{15}$ - structural and spectroscopic studies on a mixed tetrahedral-octahedral framework. *J Solid State Chem*. 2009;182:3254–61.
- Schmidmair D, Kahlenberg V, Griebner A. $\text{K}_2\text{CaSi}_4\text{O}_{10}$: a novel phase in the ternary system $\text{K}_2\text{O}-\text{CaO}-\text{SiO}_2$ and member of the litidionite group of crystal structures. *J Am Ceram Soc*. 2018;101:919–27.
- Arroyabe E, Tessadri R, Többs DM, Kahlenberg V. Does K_2CaSiO_4 exist? - a phase-analytical study in the system $\text{K}_2\text{O}-\text{CaO}-\text{SiO}_2$ with implications for the characterization of residual materials. *J Am Ceram Soc*. 2011;94:2652–5.
- Shannon RD. Revised effective ionic radii and systematic studies of interatomic distances in halides and chalcogenides. *Acta Cryst A*. 1976;32:751–67.
- Olanders B, Steenari BM. Characterization of ashes from wood and straw. *Biomass Bioenergy*. 1995;4:103–16.
- Berjonneau J, Colombel L, Poirier J, Pichavant M, Defoort F, Seiler JM. Determination of the liquidus temperatures of ashes from the biomass gazification for fuel production by thermodynamical and experimental approaches. *Energy Fuels*. 2009;23:6231–41.
- Chaivatamaset P, Sricharoon P, Tia S. Bed agglomeration characteristics of palm shell and corncob combustion in fluidized bed. *Appl Therm Eng*. 2011;31:2916–27.
- Vassilev SV, Baxter D, Vassileva CG. An overview of the behavior of biomass combustion: Part I. Phase-mineral transformations of organic and inorganic matter. *Fuel*. 2013;112:913–33.
- Boström D, Skoglund N, Grimm A, Boman C, Öhman M, Boström M, et al. Ash transformation chemistry during combustion of biomass. *Energy Fuels*. 2013;26:85–93.
- Lateef KB, Sheikh AR, Nurulakmal MS. Crystallization of potassium calcium silicate from modified industrial EAF slag. *Adv Mat Res*. 2013;620:66–71.
- Cooper GI, Cox GA. The aqueous corrosion of potash-lime-silica glass in the range 10–250°C. *Appl Geochemistry*. 1996;11:511–2.
- Doweidar H. Density-structure correlations in $\text{CaO}-\text{SiO}_2$, $\text{Na}_2\text{O}-\text{CaO}-\text{SiO}_2$ and $\text{K}_2\text{O}-\text{CaO}-\text{SiO}_2$ glasses. *Phys Chem Glasses*. 1999;40:85–9.
- Stern WB, Gerber Y. Potassium-calcium glass: new data and experiments. *Archaeometry*. 2004;46:137–56.
- Liu S, Li Q, Gan F. Chemical analyses of potash-lime silicate glass artifacts from the Warring States period in China. *Spectrosc Lett*. 2015;48:302–9.
- Yao Y, Hamada E, Sato K, Akiyama T, Yoneyama T. Identification of the major constituents of fused potassium silicate fertilizer. *ISJI Int*. 2014;54:990–3.
- Jordan MM, Almendro-Candel MB, Navarro-Pedreño J, Guirao D, Acosta A, Rincón JM. First evaluation of vitrification capability of palm tree biomass and sewage sludge. *Mater Lett*. 2018;229:71–3.
- Defoort F, Campargue M, Ratel G, Miller H, Dupont C. Physicochemical approach to blend biomass. *Energy Fuels*. 2019;33:5820–8.
- Lindberg D, Backman R, Chartrand P, Hupa M. Towards a comprehensive thermodynamic database for ash-forming elements in biomass and waste combustion - current situation and future developments. *Fuel Process Technol*. 2013;105:129–41.
- Lindberg DK, Tesfaye F, et al. The thermodynamics of slag forming inorganic phases in biomass combustion processes. In: Zhang

- L, editor. Energy Technology 2017: carbon dioxide management and other technologies. Berlin: Springer-Verlag; 2017. p. 27–41.
26. Chen M, Hou X, Chen J, Zhao B. Phase equilibria studies in the $\text{SiO}_2\text{-K}_2\text{O-CaO}$ system. *Metall Mater Trans B*. 2016;47:1690–6.
27. Santos I, Taskinen P, Jokilaakso A, Paek MK, Lindberg D. Phase equilibria and liquid behavior of the $\text{K}_2\text{O-CaO-SiO}_2$ system for entrained flow biomass gasification. *Fuel*. 2020;265:116894.
28. Hildebrandt E. Bildung und Stabilität von ausgewählten Phasen im System $\text{K}_2\text{O-CaO-SiO}_2$ und Beschreibung der neuen Phase $\text{K}_4\text{CaSi}_6\text{O}_{15}$ (in German). Master thesis, University of Innsbruck; 2021.
29. Deganello F, Tyagi AK. Solution combustion synthesis, energy and environment: best parameters for better materials. *Prog Cryst Growth Ch*. 2018;64:23–61.
30. Gates-Rector SD, Blanton TN. The powder diffraction file: a quality materials characterization database. *Powder Diffr*. 2019;34:352–60.
31. Rodriguez-Carjaval J. FullProf2.k, version 3.3, France: Laboratoire Leon Brillouin (CEA-CNRS). 2005.
32. Roisnel T, Rodriguez-Carjaval J. WinPLOTR: a windows tool for powder diffraction pattern analysis. *Mater Sci Forum*. 2001;378–381:118–24.
33. Finger LW, Cox DE, Jephcoat AP. A correction for powder diffraction peak asymmetry due to axial divergence. *J Appl Crystallogr*. 1994;27:892–900.
34. Rigaku Oxford Diffraction. CrysAlisPRO, version 1.171.40.84a. Oxford: Rigaku Oxford Diffraction; 2020.
35. Burla MC, Caliendo R, Camalli M, Carrozzini B, Cascarano GL, De Caro L, et al. SIR2004: an improved tool for crystal structure determination and refinement. *J Appl Crystallogr*. 2005;38:381–8.
36. Sheldrick GM. A short history of ShelX. *Acta Cryst A*. 2008;64:112–22.
37. Farrugia LJ. WinGX suite for small-molecule single-crystal crystallography. *J Appl Crystallogr*. 1999;32:837–8.
38. Wilson AJC (ed.) International Tables for Crystallography, Volume C. Mathematical, Physical and Chemical Tables, 1st edn. Dordrecht, Boston, London: Kluwer Academic Publishers; 1995.
39. Flack HD. On enantiomorph-polarity estimation. *Acta Crystallographica Sec A Found Crystallogr*. 1983;A39:876–81.
40. Spek AL. Single-crystal structure validation with the program PLATON. *J Appl Crystallogr*. 2003;36:7–13.
41. Robinson K, Gibbs GV, Ribbe PH. Quadratic elongation: a quantitative measure of distortion in coordination polyhedral. *Science*. 1971;172:567–70.
42. Wills AS. ValList, version 4.0.7., 2010. <http://fermat.chem.ucl.ac.uk/spaces/willsgroup/software/valist-bond-valence-calculations-listing/valist/>. Accessed December 18th. 2020.
43. Brown ID, Altermatt D. Bond-valence parameters obtained from a systematic analysis of the inorganic crystal structure database. *Acta Cryst B*. 1985;41:244–7.
44. Brese NE, O'Keeffe M. Bond-valence parameters for solids. *Acta Cryst B*. 1991;47:192–7.
45. Momma K, Izumi F. VESTA 3 for three-dimensional visualization of crystal, volumetric and morphology data. *J Appl Crystallogr*. 2011;44:1272–6.
46. Liebau F. Structural chemistry of silicates. Berlin: Springer Verlag; 1985.
47. Kahlenberg V, Rakić S, Weidenthaler C. Room- and high-temperature single crystal diffraction studies on $\gamma\text{-Na}_2\text{Si}_2\text{O}_5$: an interrupted framework with exclusively Q^3 -units. *Z Kristallogr*. 2003;218:421–31.
48. Armbruster T, Gunter ME. Crystal structures of natural zeolites. *Rev Mineral Geochem*. 2001;45:1–67.
49. Blatov VA, Shevchenko AP, Proserpio DM. Applied topological analysis of crystal structures with the program package ToposPro. *Cryst Growth Des*. 2014;14:3576–86.
50. Brunner GO, Laves F. Zum Problem der Koordinationszahl. *Wiss Z Techn Univ Dresden*. 1971;20:387–90.
51. O'Keeffe M, Peskov MA, Ramsden SJ, Yaghi OM. The Reticular Chemistry Structure Resource (RCSR) Database of, and Symbols for Crystal Nets. *Acc Chem Res*. 2008;41:1782–9.
52. Taylor HFW. Cement chemistry. London: Thomas Telford Publishing, London; 1997.
53. Angel RJ, Ross N, Seifert F, Fliervoet TF. Structural characterization of pentacoordinate silicon in a calcium silicate. *Nature*. 1996;384:441–4.
54. Morey GW, Kracek FC, Bowen NL. The ternary system $\text{K}_2\text{O-CaO-SiO}_2$: a correction. *J Soc Glass Technol*. 1931;15:57–8.
55. Kahlenberg V, Girtler D, Arroyabe E, Kaindl R, Többs DM. Devitrite ($\text{Na}_2\text{Ca}_3\text{Si}_6\text{O}_{16}$) – structural, spectroscopic and computational investigations on a crystalline impurity phase in industrial soda-lime glasses. *Mineral Petrol*. 2010;100:1–9.
56. Arroyabe E, Többs DM, Kaindl R, Kahlenberg V. Synthesis, crystal structure and vibrational spectroscopy of $\text{K}_2\text{Ca}_4\text{Si}_8\text{O}_{21}$ – an unusual single layer silicate containing Q^2 and Q^3 units. *Inorg Chem*. 2009;48:11929–34.

How to cite this article: Liu H, Hildebrandt E, Krammer H, Kahlenberg V, Krüger H, Schottenberger H. $\text{K}_4\text{CaSi}_6\text{O}_{15}$ —Solving a 90-year-old riddle. *J Am Ceram Soc*. 2021;00:1–18. <https://doi.org/10.1111/jace.17920>